Water Resources Research

RESEARCH ARTICLE
10.1029/2022WR032215

Spatial Markov Model for the Prediction of Travel-Time-Based Solute Dispersion in Three-Dimensional Heterogeneous Media

Olaf A. Cirpka[1], Marie-Madeleine Stettler[1], and Marco Dentz[2]

[1]Center for Applied Geoscience, University of Tübingen, Tübingen, Germany, [2]Spanish National Research Council (CSIC), Institute of Environmental Assessment and Water Research (IDÆA), Barcelona, Spain

Key Points:

- We derive closed-form expressions of ensemble dispersion in the spatial-Markov framework of solute transport
- The expressions are consistent with linear theory in the limit of small log-conductivity variances, but extend to high-variance cases
- Comparison to particle-tracking simulations of advective transport in 3-D heterogeneous domains show excellent agreement

Correspondence to:
O. A. Cirpka,
olaf.cirpka@uni-tuebingen.de

Citation:
Cirpka, O. A., Stettler, M.-M., & Dentz, M. (2022). Spatial Markov Model for the prediction of travel-time-based solute dispersion in three-dimensional heterogeneous media. *Water Resources Research*, *58*, e2022WR032215. https://doi.org/10.1029/2022WR032215

Received 17 FEB 2022
Accepted 27 MAY 2022

Abstract In recent years, Spatial Markov Models have gained popularity in simulating solute transport in heterogeneous formations. They describe the transition times of particles between equidistant observation planes by statistical distributions, assuming correlation of the transit times of individual particles between subsequent steps. By this, the approach naturally captures preasymptotic solute dispersion. In this study, we analyze Spatial Markov Models assuming bivariate log-normal distributions of the particle slowness (i.e., the inverse velocity) in subsequent transitions. The model is fully parameterized by the mean Eulerian velocity, the variance of the log-slowness, and the correlation coefficient of log-slowness in subsequent steps. We derive closed-form expressions for distance-dependent ensemble dispersion, which is defined in terms of the second-central moments of the solute breakthrough curves. We relate the coefficients to the properties of the underlying log-hydraulic conductivity field assuming second-order stationarity. The results are consistent with linear stochastic theory in the limit of small log-conductivity variances, while the approach naturally extends to high-variance cases. We demonstrate the validity of the approach by comparison to three-dimensional particle-tracking simulations of advective transport in heterogeneous media with isotropic, exponential correlation structure for log-conductivity variances up to five. This study contributes to relating solute dispersion to metrics of the porous-medium structure in cases of strong heterogeneity.

1. Introduction

The adequate parameterization of solute transport in natural, inherently heterogeneous formations has been the subject of intensive research in hydrogeology and environmental engineering over the last four decades. Classical Fickian macrodispersion concepts, parameterizing the effects of unresolved spatial variability on field-scale transport by a diffusion-type macrodispersion term with constant coefficients, can neither reproduce the evolution of solute spreading over shorter distances and travel times nor can it predict long tailing observed in field investigations (e.g., Adams & Gelhar, 1992; Haggerty et al., 2001; Kang et al., 2015). First-order perturbative approaches, typically assuming second-order stationary multi-Gaussian log-hydraulic conductivity ($\ln K$) fields and uniform-in-the-mean hydraulic gradients, are good in predicting second-central spatial moments of solute plumes as long as the variance of $\ln K$ remains small (Gelhar & Axness, 1983; Dagan, 1984; Dentz et al., 2000; Fiori, 2001; Neuman et al., 1987, among others). These techniques have been transferred to the prediction of temporal moments of solute plumes passing observation planes (e.g., Cvetkovic et al., 1992, 1996; Shapiro & Cvetkovic, 1988). The perturbative approaches are not only limited to small variances of $\ln K$, but also fall short of predicting full spatial concentration profiles or breakthrough curves without additional assumptions, because they exclusively target concentration moments. Conversely, they offer a rigorous framework to relate properties of the formation and the mean flow field to metrics of solute spreading.

Alternative parameterizations of field-scale solute transport in heterogeneous formations include (a) the fractional advection-dispersion equation, involving non-integer spatial and/or temporal derivatives (e.g., Benson et al., 2000), (b) multi-continuum approaches, assuming overlapping continua with different mobility (e.g., Ahmadi et al., 1998; Cherblanc et al., 2003; Haggerty & Gorelick, 1995; Li et al., 2011), (c) Time-Domain Random Walk (TDRW) models, parameterizing uncorrelated travel-time distributions between observation planes (e.g., Cvetkovic et al., 2014), and (d) Continous-Time Random-Walk (CTRW) formulations, in which spatial random walks are combined with random waiting-time distributions (e.g., Berkowitz et al., 2006; Berkowitz & Scher, 1997), see also the review by Noetinger et al. (2016). Despite success reports on fitting these models to observed breakthrough curves, it remains a challenge to derive the coefficients appearing in these parameterizations from properties of the formation and large-scale boundary conditions.

A key assumption of standard TDRW and CTRW formulations is that individual random-walk steps are uncorrelated. Le Borgne et al. (2008) introduced a variant of TDRW or CTRW, in which transition times, or particle velocities, between fixed observation planes are modeled as first-order Markov processes. We refer to this model in the following as Spatial Markov Model (Sherman et al., 2021) because the transition time and velocity of particles evolve with spatial distance instead of time. In essence, the slowness (i.e., the inverse velocity, e.g., Gotovac et al., 2009) of a solute particle, and thus the time increment from one observation plane to the next, is considered a first-order Markov process, in which the current time increment is conditioned on the preceding one. The approach requires either a transition matrix, that is, a discrete joint distribution of two consecutive stepsizes (Le Borgne et al., 2008), or a parametric model serving the same purpose. Massoudieh et al. (2017) compared joint distributions with three different (log-normal, truncated power-law, and Levy) marginal distributions and a Gaussian copula to describe the statistical dependence. The latter implies that a normal-score transformation of the marginal distributions lead to a bivariate normal distribution. Morales et al. (2017) used a bivariate log-normal distribution of particle speeds with a Gaussian copula to model pore-scale particle motion from particle tracking data in a three-dimensional porous medium. Dentz et al. (2020) used the skewed log-normal distribution with a Gaussian copula. Restricting to a bivariate log-normal distribution, however, does not only agree fairly well with numerically obtained velocity distributions in multi-Gaussian log-conductivity fields (e.g., Englert et al., 2006; Nowak et al., 2008), but also has convenient properties outlined in Appendix A. The present study analyzes properties of CTRW and TDRW based on a Spatial Markov Model using the bivariate log-normal distribution in order to predict travel-time-based solute dispersion.

Dentz et al. (2016) and Morales et al. (2017) proposed explicit analytical Markov models for the evolution of particle speeds and thus travel time increments for purely advective transport that have been employed to predict large-scale transport in highly heterogeneous porous and fractured media (Comolli et al., 2019; Hyman & Dentz, 2021; Puyguiraud et al., 2019). Spatial Markov Models naturally generate the evolution of solute spreading. Because random-walk simulations of the spatial Markov process are computationally very efficient, full breakthrough curves can easily be generated by following a sufficiently large ensemble of particles. Recently, Sherman et al. (2021) reviewed the original development, applications and extensions of the approach.

Like in many preceding studies, we will neglect local dispersion in the present analysis. Upon this restriction, the Lagrangian velocity of a single particle at a given point is identical to the corresponding Eulerian velocity at that point. Local dispersion is known to affect longitudinal ensemble dispersion only to a small extent (e.g., Dagan & Fiori, 1997). This is different for effective dispersion of plumes related to a point injection, for which Spatial Markov Models have not been developed.

The present contribution takes a closer look onto Spatial Markov Models characterized by bivariate log-normal distributions of successive travel-time steps. In particular, we derive analytical expressions of the mean arrival time and travel-time based ensemble dispersion for flux- and volume-weighted injections. We also analyze how well the approach compares to numerical simulations of advective transport in 3-D heterogeneous domains with isotropic correlation structure of the log-hydraulic conductivity field, attempting to relate the coefficients of the Spatial Markov Model to parameters describing the variability of the log-conductivity field.

2. Theory

2.1. Spatial Markov Process

In CTRW or TDRW approaches, the movement of a particle is described in spatial increments of Δx in the direction of mean flow by the following updating rule (Le Borgne et al., 2008):

$$x_{i+1} = x_i + \Delta x, \tag{1}$$

$$\tau_{i+1} = \tau_i + \alpha_i \Delta x, \tag{2}$$

in which $\alpha_i = \alpha(x_i)$ is the slowness, that is, the inverse particle velocity $u(x_i)$ in the direction of mean flow, experienced by the particle at location x_i:

$$\alpha(x_i) = \frac{1}{u(x_i)}, \tag{3}$$

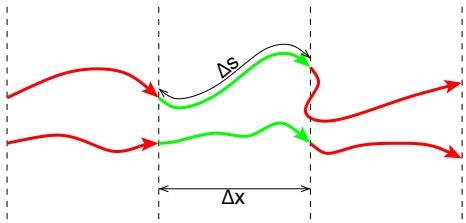

Figure 1. Illustration of particle trajectories. While the true trajectories are tortuous with path length Δs_i over segment i, the Spatial Markov Model considers only the distance Δx in the longitudinal direction. The effective velocity u is given by dividing the velocity along the path by the ratio $\chi = \Delta s/\Delta x$.

The effective particle velocity in direction x is $u(x_i) = \overline{\|\mathbf{v}(x_i)\|_2}/\chi$, where $\mathbf{v}(x_i)$ is the true velocity vector of the particle, the overline denotes averaging over the path segment, and χ is the advective tortuosity (Puyguiraud et al., 2019). Figure 1 illustrates the principle. In cases in which the path-velocity component in direction x is locally negative, the approach considers the time until first arrival at an observation plane. By this, u is always positive. In Section 3, we discuss how we estimate the tortuosity of a velocity field without following individual trajetories.

The effective particle speed u_i in direction x is expressed by a first-order Markov process, denoted spatial Markov process. This implies that in subsequent CTRW/TDRW steps, the slowness α_{i+1} is drawn from the conditional distribution $p_{i+1,i}(\alpha|\alpha')$ where α' is the value of α_i in the previous step. The conditional distribution satisfies the Chapman-Kolmogorov equation:

$$p_{i,j}\left(\alpha|\alpha'\right) = \int_0^\infty p_{i,k}\left(\alpha|\alpha''\right) p_{k,j}\left(\alpha''|\alpha'\right) d\alpha'' \tag{4}$$

for $i > k > j$. The joint distribution of α_i and α_j is given by $p_{i,j}(\alpha, \alpha') = p_{i,j}(\alpha|\alpha')p_j(\alpha')$, where $p_j(\alpha')$ is the distribution of slowness after j steps. From this, we obtain the evolution of the distribution $p_i(\alpha)$ with increasing number of steps, or equivalently with increasing spatial distance, from an initial distribution $p_0(\alpha)$:

$$p_i(\alpha) = \int_0^\infty p_{i,0}\left(\alpha|\alpha'\right) p_0\left(\alpha'\right) d\alpha'. \tag{5}$$

At a sufficiently large travel distance for transport in a stationary velocity field, typically much larger than the correlation length of the $\ln K$-field, $p_i(\alpha)$ converges toward the asymptotic distribution $p_\infty(\alpha)$. That is, if the initial distribution $p_0(\alpha)$ equals the asymptotic distribution $p_\infty(\alpha)$, the distribution $p_i(\alpha)$ of particle slowness remains $p_\infty(\alpha)$ in all steps. If the initial distribution $p_0(\alpha) \neq p_\infty(\alpha)$, then $p_i(\alpha)$ evolves toward $p_\infty(\alpha)$ according to Equation 5.

The distribution $p_i(\alpha)$ is related to the distribution $p_i^u(u)$ of particle velocities at step i through $p_i(\alpha) = p_i^u(1/\alpha)/\alpha^2$ because $\alpha = 1/u$. The asymptotic distribution of flow velocities is denoted by $p_f(u)$ such that $p_\infty(\alpha) = p_f(1/\alpha)/\alpha^2$. As the fluid flux arranges itself to be concentrated in high-velocity regions, the distribution $p_f(u)$ is given by the flux-weighted (effective) Eulerian velocity distribution (Dentz et al., 2016):

$$p_f(u) = \frac{u}{\mu_{v,u}} p_v(u), \tag{6}$$

where $p_v(u)$ denotes the (effective) Eulerian velocity distribution and $\mu_{v,u}$ its mean. The subscript f refers to flux-weighting. The subscript v refers to the fact that the Eulerian velocity distribution is obtained by volumetric sampling. From these considerations, we see that the mean slowness in this asymptotic limit is $\mu_\alpha = 1/\mu_{v,u}$.

We consider here two injection modes: flux- and volume-weighted. For a flux-weighted injection, the initial velocity distribution equals the asymptotic distribution $p_f(u)$. This implies that the distribution $p_i(\alpha)$ of α_i equals the asymptotic distribution $p_\infty(\alpha)$. For the volume-weighted injection, the initial velocity distribution equals the Eulerian distribution $p_v(u)$. In this case, the initial distribution $p_0(\alpha)$ of α_0 is not stationary, and the slowness statistics $p_i(\alpha)$ evolve according to Equation 4 as outlined above.

In the following, we normalize the effective velocity u, slowness α, distance x, and time t with the mean Eulerian velocity $\mu_{v,u}$, and a characteristic length of the formation, which we set to the integral scale $\lambda_{\ln K}$ of log-hydraulic conductivity variations within that formation:

$$u_* = \frac{u}{\mu_{v,u}}, \qquad \alpha_* = \alpha\mu_{v,u}, \qquad x_* = \frac{x}{\lambda_{\ln K}}, \qquad t_* = \frac{t\mu_{v,u}}{\lambda_{\ln K}}, \tag{7}$$

in which properties with an asterisk are dimensionless. For simplicity of notation, we drop the asterisks in the following. Upon this normalization, the mean asymptotic slowness equals one, $\mu_\alpha = 1$.

2.2. Bivariate Log-Normal Distribution

2.2.1. Velocities

Many theoretical and numerical studies assume a log-normal distribution of hydraulic conductivity. As the local Eulerian velocity is the hydraulic conductivity times the local hydraulic gradient divided by the porosity, deviations of the Eulerian velocity distribution from the log-normal case result from the interactions between the log-conductivity variations and hydraulic-gradient variations. These deviations have been found small in numerical studies (e.g., Dentz et al., 2020; Englert et al., 2006; Nowak et al., 2008). We thus make the conceptual choice that the effective Eulerian velocity distribution is log-normal:

$$p_v(u) = \frac{1}{u\sqrt{2\pi\sigma^2_{\ln u}}} \exp\left(-\frac{(\ln u - \mu_{v,\ln u})^2}{2\sigma^2_{\ln u}}\right), \tag{8}$$

where $\mu_{v,\ln u}$ and $\sigma^2_{\ln u}$ are the mean and variance of the log-Eulerian velocity. Then the mean and variance of the non-logarithmic Eulerian velocity are given by:

$$\mu_{v,u} = \exp\left(\mu_{v,\ln u} + \frac{\sigma^2_{\ln u}}{2}\right) = 1, \tag{9}$$

$$\sigma^2_{v,u} = \left(\exp\left(\sigma^2_{\ln u}\right) - 1\right) \exp\left(2\mu_{v,\ln u} + \sigma^2_{\ln u}\right) = \exp\left(\sigma^2_{\ln u}\right) - 1. \tag{10}$$

Note that Equation 9 implies that $\mu_{v,\ln u} = -\sigma^2_{\ln u}/2$. Conversely, the moments of the log-Eulerian velocity can be expressed in terms of the mean $\mu_{v,u}$ and variance $\sigma^2_{v,u}$ of the non-logarithmic Eulerian velocity by (e.g., Zerovnik et al., 2013):

$$\mu_{v,\ln u} = \ln\left(\frac{\mu^2_{v,u}}{\sqrt{\sigma^2_{v,u} + \mu^2_{v,u}}}\right) = \ln\left(\frac{1}{\sqrt{\sigma^2_{v,u} + 1}}\right), \tag{11}$$

$$\sigma^2_{\ln u} = \ln\left(\frac{\sigma^2_{v,u}}{\mu^2_{v,u}} + 1\right) = \ln\left(\sigma^2_{v,u} + 1\right). \tag{12}$$

As outlined in Appendix A, the fact that $p_v(u)$ is log-normal implies that the flux-weighted velocity distribution $p_f(u)$ is also log-normal with:

$$\mu_{f,\ln u} = \mu_{v,\ln u} + \sigma^2_{\ln u} = \frac{\sigma^2_{\ln u}}{2} = -\mu_{v,\ln u}. \tag{13}$$

The mean and variance $\mu_{f,u}$ and $\sigma^2_{f,u}$ of the flux-weighted velocity distribution $p_f(u)$ are then given by (e.g., Zerovnik et al., 2013):

$$\mu_{f,u} = \exp\left(\mu_{f,\ln u} + \frac{\sigma^2_{\ln u}}{2}\right) = \exp\left(\sigma^2_{\ln u}\right), \tag{14}$$

$$\sigma^2_{f,u} = \left(\exp\left(\sigma^2_{\ln u}\right) - 1\right) \exp\left(2\mu_{f,\ln u} + \sigma^2_{\ln u}\right) = \left(\exp\left(\sigma^2_{\ln u}\right) - 1\right) \exp\left(2\sigma^2_{\ln u}\right). \tag{15}$$

In the asymptotic limit, we assume that the joint distribution $p^u_{i,j}(u, u')$ of Lagrangian velocities $u_i = u$ and $u_j = u'$ in steps i and j, respectively, is the bivariate log-normal distribution (e.g., Zerovnik et al., 2013) with the flux-weighted velocity distribution $p_f(u)$ as the marginal distribution of both u_i and u_j:

$$p^u_{i,j}(u, u') = \frac{1}{2\pi u u' \sigma^2_{\ln u}\sqrt{1 - r^2_{i,j}}} \cdot \exp\left(-\frac{1}{2\sigma^2_{\ln u}} \left[\ln u - \mu_{f,\ln u},\ \ln u' - \mu_{f,\ln u}\right] \begin{bmatrix} 1 & r_{i,j} \\ r_{i,j} & 1 \end{bmatrix}^{-1} \begin{bmatrix} \ln u - \mu_{f,\ln u} \\ \ln u' - \mu_{f,\ln u} \end{bmatrix}\right), \tag{16}$$

where $r_{i,j}$ denotes the correlation coefficient between steps i and j, and square brackets, $[\cdot]$, denote vectors and matrices. The use of a bivariate log-normal distribution for the particle velocities is equivalent to representing the series of log-velocities by an Ornstein-Uhlenbeck process as done in Morales et al. (2017), which follows Gaussian statistics. According to the Doob theorem (Doob, 1942), any stationary Gaussian process is necessarily an Ornstein-Uhlenbeck process, which motivates the use of the bivariate log-normal distribution here.

Consistently, the conditional distribution $p^u_{i,j}(u|u')$ of the velocity $u_i = u$ of a single particle in step i, given that its velocity in step j is $u_j = u'$, equals the conditional log-normal distribution:

$$p^u_{i,j}\left(u|u'\right) = \frac{1}{u\sqrt{2\pi\sigma^2_{\ln u}\left(1-r^2_{i,j}\right)}}\exp\left(-\frac{\left(\ln u - \mu_{f,\ln u} - \left(\ln u' - \mu_{f,\ln u}\right) r_{i,j}\right)^2}{2\sigma^2_{\ln u}\left(1-r^2_{i,j}\right)}\right), \tag{17}$$

The Chapman-Kolmogorov Equation 4 requires that $r_{i,j} = r_{i,k}r_{k,j}$ is independent of k. This implies that $r_{i,j} = r_0^{i-j}$, in which r_0 is the correlation coefficient of a single transition. We can associate r_0, which depends on the step-size Δx of a single transition, to the integral scale $\lambda_{\ln u}$ of $\ln u(x)$, which is independent of the discretization:

$$r_0 = \exp\left(-\frac{\Delta x}{\lambda_{\ln u}}\right). \tag{18}$$

Note that the joint distribution of Equation 16 is formulated for the asymptotic limit at which the velocity distribution of all particles does not change anymore upon transitions, whereas the conditional distribution $p^u_{i,j}(u|u')$ of Equation 17 does not require a particular distribution of the particle velocity at the preceding step j. However, Equation 17 and $r_{i,j} = r_0^{i-j}$ guarantee that, after many transitions, the Lagrangian velocity distribution approaches the asymptotic distribution $p_f(u)$, regardless of the initial distribution. This is evident as $r_{i,j}$ converges toward zero for $i \gg j$, so that $p^u_{i,j}(u|u')$ becomes independent of u' and converges toward $p_f(u)$.

2.2.2. Slowness

As the slowness is the inverse of the particle velocity, its asymptotic distribution $p_\infty(\alpha)$ is also log-normally distributed, where the mean and variance $\mu_{\ln\alpha}$ and $\sigma^2_{\ln\alpha}$ are given by.

$$\mu_{\ln\alpha} = -\mu_{f,\ln u} - \frac{\sigma^2_{\ln u}}{2} = \mu_{v,\ln u}, \tag{19}$$

$$\sigma^2_{\ln\alpha} = \sigma^2_{\ln u}. \tag{20}$$

This property of the log-normal distribution implies that the asymptotic distribution $p_\infty(\alpha)$ of the normalized slowness is identical to the volume-weighted Eulerian velocity distribution. The mean and variance of $p_\infty(\alpha)$ are then given by:

$$\mu_\alpha = 1, \tag{21}$$

$$\sigma^2_\alpha = \sigma^2_{v,u}, \tag{22}$$

and the conditional distribution of the slowness is given by:

$$p_{i,j}\left(\alpha|\alpha'\right) = \frac{1}{\alpha\sqrt{2\pi\sigma^2_{\ln u}\left(1-r_0^{2(i-j)}\right)}}\exp\left(-\frac{\left(\ln\alpha - \mu_{f,\ln u} - \left(\ln\alpha' - \mu_{f,\ln u}\right) r_0^{i-j}\right)^2}{2\sigma^2_{\ln u}\left(1-r^{2(i-j)}\right)}\right), \tag{23}$$

As outlined above, for a flux-weighted injection, the initial distribution $p_0(\alpha)$ of slowness equals its asymptotic distribution $p_\infty(\alpha)$. For a uniform injection into the volume, by contrast, the initial distribution $p_0(\alpha)$ is log-normal with:

$$\mu_{0,\ln\alpha} = -\mu_{v,\ln u}, \tag{24}$$

$$\sigma^2_{0,\ln\alpha} = \sigma^2_{\ln u}. \tag{25}$$

That is, in case of a volume-weighted injection the initial distribution of the slowness is identical to the flux-weighted Eulerian velocity distribution. Again a property of the log-normal distribution.

2.2.2.1. Mean

The mean slowness is defined by:

$$\langle \alpha_i \rangle = \int_0^\infty \alpha p_i(\alpha) d\alpha, \tag{26}$$

where $p_i(\alpha)$ is given by Equation 5. The angular brackets, $\langle \cdot \rangle$, denote the average over all particles. In case of a flux-weighted injection, the initial distribution $p_0(\alpha)$ equals the asymptotic distribution $p_\infty(\alpha)$, and so does $p_i(\alpha)$ in all steps i. Under this condition, the mean slowness $\langle \alpha_i \rangle$ is unity in all steps. If the initial distribution is also log-normal with identical variance of the log-slowness, namely $\sigma^2_{\ln u}$, but different mean $\mu_{\ln\alpha_0}$, then $p_i(\alpha)$ is also log-normal, with the same variance $\sigma^2_{\ln u}$ and the following mean $\mu_{\ln\alpha_i}$ of $\ln\alpha_i$:

$$\mu_{\ln\alpha_i} = \mu_{v,\ln u} + \left(\mu_{\ln\alpha_0} - \mu_{v,\ln u}\right) r_0^i. \tag{27}$$

The mean slowness is then given by:

$$\langle \alpha_i \rangle = \exp\left(\mu_{\ln\alpha_i} + \frac{\sigma^2_{\ln u}}{2}\right). \tag{28}$$

2.2.2.2. Covariance

The covariance C_{ij} of slowness at steps i and j is defined in terms of the marginal distribution $p_j(\alpha)$ of α_j and the conditional probability $p_{ij}(\alpha|\alpha')$ as:

$$C_{ij} = \int_0^\infty \int_0^\infty \left(\alpha - \langle \alpha_i \rangle\right)\left(\alpha' - \langle \alpha_j \rangle\right) p_{ij}\left(\alpha|\alpha'\right) p_j\left(\alpha'\right) d\alpha' d\alpha. \tag{29}$$

where $i > j$. If $p_j(\alpha)$ is log-normally distributed with the same log-variance $\sigma^2_{\ln u}$ as the asymptotic distribution, C_{ij} is given by (e.g., Zerovnik et al., 2013):

$$C_{ij} = \exp\left(\mu_{\ln\alpha_i} + \mu_{\ln\alpha_j} + \sigma^2_{\ln u}\right)\left(\exp\left(\sigma^2_{\ln u} r_0^{i-j}\right) - 1\right). \tag{30}$$

where $\mu_{\ln\alpha_i}$ is the mean of $\ln\alpha_i$. Under stationary conditions $\mu_{\ln\alpha_i} = \mu_{\ln\alpha_j} = -\sigma^2_{\ln u}/2$. In this case, the covariance function reduces to:

$$C_{ij} = \exp\left(\sigma^2_{\ln u} r_0^{i-j}\right) - 1. \tag{31}$$

2.3. Mean Travel Time and Travel-Time Based Ensemble Dispersion

We derive here expressions for the mean and variance of travel time, and the travel-time based ensemble dispersion coefficient. We consider flux- and volume-weighted injection modes, with $\mu_{0,\ln\alpha} = \mu_{v,\ln u}$ and $\mu_{0,\ln\alpha} = -\mu_{v,\ln u}$, respectively. In both cases the variance of log-slowness equals $\sigma^2_{\ln u}$.

The mean and variance of travel time after n steps are defined by:

$$\mu_{\tau_n} = \sum_{i=0}^{n-1} \Delta x \langle \alpha_i \rangle, \tag{32}$$

$$\sigma^2_{\tau_n} = \sum_{i=0}^{n-1} \Delta x \sum_{j=0}^{n-1} \Delta x \langle (\alpha_i - \langle \alpha_i \rangle)(\alpha_j - \langle \alpha_j \rangle) \rangle = 2 \sum_{i=0}^{n-1} \Delta x \sum_{j=0}^{i} \Delta x C_{ij}. \tag{33}$$

In order to evaluate these expressions, we perform the continuum limit $\Delta x \to 0$ and $n \to \infty$ such that $x_n = n\Delta x \to x$ is finite. In this limit we obtain:

$$\mu_\tau(x) = \int_0^x \mu_\alpha \left(x'\right) dx', \tag{34}$$

where we set $\mu_{\tau_n} \to \mu_\tau(x)$ and $\langle \alpha_i \rangle \to \mu_\alpha(x)$. In the continuum limit, the variance of the travel time is given by:

$$\sigma^2_\tau(x) = 2 \int_0^x \int_0^{x'} C\left(x', x''\right) dx'' dx', \tag{35}$$

where we set $C_{ij} \to C(x', x'')$. Furthermore, we set $r^i_0 \to \exp\left(-x/\lambda_{\ln u}\right)$, where we used the definition of Equation 18. Equations 34 and 35 were formulated by Shapiro and Cvetkovic (1988) and have been analyzed using first-order analytical expressions of the Eulerian velocity (e.g., Cvetkovic et al., 1992; Gotovac et al., 2009) and non-linear extensions thereof (Cvetkovic et al., 1996) in the past. The difference between these results and our analysis is that we assume the log-slowness to be bivariate normal distributed with exponential covariance function instead of relying on first-order results of the Eulerian, non-logarithmic velocity.

The travel-time based ensemble dispersion coefficient $D(x)$ is defined by:

$$D(x) \equiv \frac{1}{2} \frac{d\sigma^2_\tau(x)}{dx} \left(\frac{d\mu_\tau(x)}{dx} \right)^{-3}. \tag{36}$$

Using Equations 34 and 35 we obtain:

$$D(x) = \frac{1}{\mu^3_\alpha(x)} \int_0^x C\left(x, x''\right) dx''. \tag{37}$$

2.3.1. Flux-Weighted Injection

We consider the case that solute particles are introduced proportional to the volume flux at locations with longitudinal coordinate $x_0 = 0$. Under this condition, $\mu_\alpha(x) = 1$ and the covariance is given by the continuum limit of Equation 31 as:

$$C\left(x, x'\right) = C\left(x - x'\right) \equiv \exp\left(\sigma^2_{\ln u} \exp\left(-\left(x - x'\right)/\lambda_{\ln u}\right)\right) - 1. \tag{38}$$

Thus, we obtain from Equations 34 and 37:

$$\mu_\tau(x) = x, \tag{39}$$

$$D(x) = \int_0^x \left(\exp\left(\sigma^2_{\ln u} \exp\left(-x'/\lambda_{\ln u}\right)\right) - 1\right) dx'. \tag{40}$$

Performing the integration in Equation 37 gives for $D(x)$:

$$D(x) = \lambda_{\ln u} \left(\left(\mathrm{Ei}\left(\sigma^2_{\ln u}\right) - \mathrm{Ei}\left(\sigma^2_{\ln u} \exp\left(-\frac{x}{\lambda_{\ln u}}\right)\right)\right) - \frac{x}{\lambda_{\ln u}} \right), \tag{41}$$

with the exponential integral $\mathrm{Ei}(z) = \int_{-\infty}^{z} \frac{\exp(\zeta)}{\zeta} d\zeta$.

In the limits of $x \to 0$ and $x \to \infty$, we obtain:

$$\lim_{x \to 0} D(x) = x\left(\exp\left(\sigma^2_{\ln u}\right) - 1\right) = x\sigma^2_{v,u}, \tag{42}$$

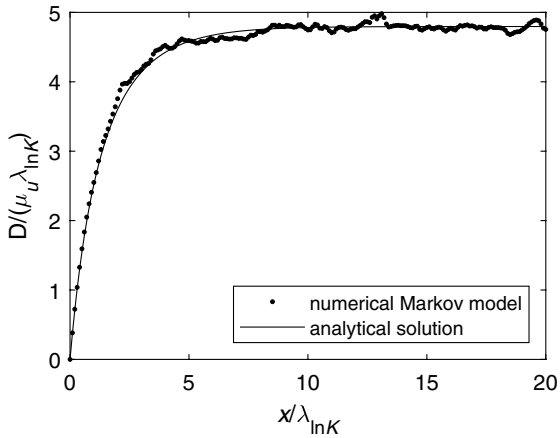

Figure 2. Travel-time-based dimensionless dispersion coefficient for injection into the flux. Comparison between numerical simulation of a Spatial Markov Model and Equation 41. $\sigma^2_{\ln u} = 1.6$, $\lambda_{\ln u} = 1.875\lambda_{\ln K}$, $\Delta x = 0.1\lambda_{\ln K}$, number of particles: 10^6.

$$D_\infty = \lim_{x\to\infty} D(x) = \left(\mathrm{Ei}\left(\sigma^2_{\ln u}\right) - \ln\left(\sigma^2_{\ln u}\right) - \gamma\right)\lambda_{\ln u} = \left(\sum_{n=1}^{\infty} \frac{\sigma^{2n}_{\ln u}}{nn!}\right)\lambda_{\ln u} \approx \left(\sigma^2_{\ln u} + \frac{\sigma^4_{\ln u}}{4} + \frac{\sigma^6_{\ln u}}{18} + \frac{\sigma^8_{\ln u}}{96}\right)\lambda_{\ln u}, \tag{43}$$

where $\gamma \approx 0.57722$ is the Euler-Mascheroni constant. Note that this non-linear expression of ensemble dispersion differs from the non-linear extension of first-order results presented by Cvetkovic et al. (1996). For small values of $\sigma^2_{\ln u}$, Equation 41 approaches the first-order result at the limits $x \to 0$ and $x \to \infty$.

Figure 2 shows a comparison of numerical results for the evolution of the dimensionless dispersion coefficient applying the Spatial Markov Model with one million particles injected into the flux and Equation 41, confirming the validity of the analytical expression. Note that, while the calculations are performed in dimensionless form, we explicitly report the normalizations of the corresponding dimensional terms in the axis labels and captions in this and the following figures to increase the comprehensibility of the plots without reading the entire article.

2.3.2. Volume-Weighted Injection

In case of a volume-weighted injection, the initial distribution $p_0(\alpha) = p_f(u)$ of the slowness of particles differs from the asymptotic distribution $p_\infty(\alpha) = p_v(u)$. Both $p_0(\alpha)$ and $p_\infty(\alpha)$ are log-normally distributed. They have the same variance $\sigma^2_{\ln u}$ but different mean values of log-slowness, namely $\mu_{f,\ln u}$ and $\mu_{v,\ln u}$, respectively. Thus, the evolution of the mean slowness is given in the continuum limit of Equation 28 as:

$$\mu_\alpha(x) = \exp\left(\sigma^2_{\ln u}\exp\left(-\frac{x}{\lambda_{\ln u}}\right)\right), \tag{44}$$

where we have used that $\mu_{\ln\alpha}(0) = \mu_{f,\ln u}$ and Equation 13. Using this expression in the definition of the mean travel time, Equation 34, and performing the integration gives:

$$\mu_\tau(x) = \lambda_{\ln u}\left(\mathrm{Ei}\left(\sigma^2_{\ln u}\right) - \mathrm{Ei}\left(\sigma^2_{\ln u}\exp\left(-\frac{x}{\lambda_{\ln u}}\right)\right)\right). \tag{45}$$

In order to determine the ensemble dispersion coefficient according to Equation 37, we consider the continuum limit of the covariance function defined by Equation 30:

$$C\left(x, x'\right) = \exp\left(\mu_{\ln\alpha}(x) + \mu_{\ln\alpha}\left(x'\right) + \sigma^2_{\ln u}\right)\left(\exp\left(\sigma^2_{\ln u}\exp\left(-\left(x - x'\right)/\lambda_{\ln u}\right)\right) - 1\right), \tag{46}$$

where we have set $\mu_{\ln\alpha_i} \to \mu_{\ln\alpha}(x)$, and Equation 18 for r_0. The mean $\mu_{\ln\alpha}(x)$ of the log-slownes is given by the continuum limit of Equation 27 as:

$$\mu_{\ln\alpha}(x) = \sigma^2_{\ln u}\left(\exp\left(-x/\lambda_{\ln u}\right) - \frac{1}{2}\right), \tag{47}$$

where we have used that $\mu_{\ln\alpha}(0) = \mu_{f,\ln u}$ and Equation 13. Substituting Equation 47 into Equation 46 gives:

$$C\left(x, x'\right) = \exp\left(\sigma^2_{\ln u}\left(\exp\left(-x/\lambda_{\ln u}\right) + \exp\left(-x'/\lambda_{\ln u}\right)\right)\right)\left(\exp\left(\sigma^2_{\ln u}\exp\left(-\left(x - x'\right)/\lambda_{\ln u}\right)\right) - 1\right). \tag{48}$$

The dispersion coefficient defined by Equation 37 is now given by:

$$D(x) = \frac{\int_0^x \exp\left(\sigma^2_{\ln u}\left(\exp\left(-x/\lambda_{\ln u}\right) + \exp\left(-x'/\lambda_{\ln u}\right)\right)\right)\left(\exp\left(\sigma^2_{\ln u}\exp\left(-\left(x - x'\right)/\lambda_{\ln u}\right)\right) - 1\right)dx'}{\exp\left(3\sigma^2_{\ln u}\exp\left(-\frac{x}{\lambda_{\ln u}}\right)\right)}. \tag{49}$$

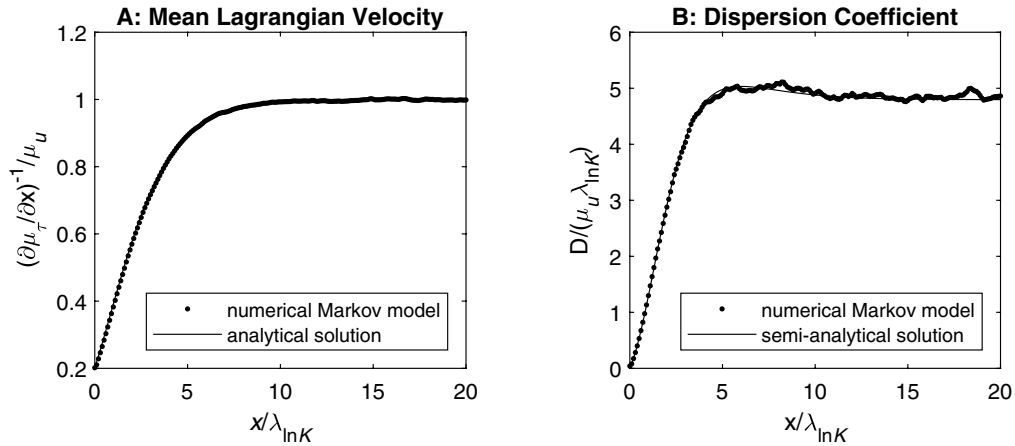

Figure 3. Travel-time-based dimensionless Lagrangian velocity and dispersion coefficient for injection into the volume. Comparison between numerical simulation of a Spatial Markov Model and Equations 45 and 49. $\sigma^2_{\ln u} = 1.6$, $\lambda_{\ln u} = 1.875\lambda_{\ln K}$, $\Delta x = 0.1\lambda_{\ln K}$, number of particles: 10^6.

To the best of our knowledge, the integral in the nominator does not have a closed-form solution, so that it needs to be evaluated numerically.

At short distances, $x \to 0$, we obtain for the mean travel time from Equation 45:

$$\lim_{x\to 0} \mu_\tau(x) = \exp\left(\sigma^2_{\ln u}\right) x = \mu_{f,u} x. \tag{50}$$

In the same limit, we obtain for the dispersion coefficient $D(x)$:

$$\lim_{x\to 0} D(x) = \left(1 - \exp\left(-\sigma^2_{\ln u}\right)\right) x. \tag{51}$$

Figure 3 shows a comparison of numerical results for the evolution of the dimensionless Lagrangian velocity (i.e., the inverse slowness), and dispersion coefficient applying the Spatial Markov Model with one million particles injected into the volume and the numerical integration of Equation 49. In contrast to the case with injection into the flux, there is a tiny offset in the evolution of the mean Lagrangian velocity between the numerical and analytical results, which can be attributed to the explicit-Euler type of integration applied to the evolution of $\mu_{\ln\alpha}$ when performing the discrete Spatial Markov Model, in contrast to the exact integration in the analytical result underlying Equation 45. Similarly, we observe tiny differences in the evolution of the dispersion coefficient.

3. Comparison to 3-D Particle-Tracking Simulations in Isotropic Heterogeneous Media

We test the validity of the Spatial Markov Model assuming a bivariate log-normal distribution of travel-time increments for advective solute transport in flow fields resulting from auto-correlated heterogeneous hydraulic-conductivity fields. Toward this end, we perform flow and particle-tracking simulations in 3-D periodic domains with isotropic, exponential covariance functions of the scalar log-hydraulic conductivity using multiple random realizations of the log-conductivity field. The domain has dimensions ($L \times W \times H$) of $40 \times 20 \times 20$ integral scales $\lambda_{\ln K}$ of $\ln K$-variations. The spatial discretization of the periodic fields is $0.1\lambda_{\ln K}$ in all directions. The fields are generated by the spectral approach of Dietrich and Newsam (1993). We simulate groundwater flow by a cell-centered Finite Volume method, applying periodic boundary conditions with differences in the mean hydraulic head at opposing faces such that the mean specific-discharge is exactly oriented in the longitudinal x-direction. We solve the resulting systems of linear equations by the preconditioned conjugate gradient method with algebraic multigrid preconditioning (e.g., Stüben, 2001), implemented in the HSL-MI20 library (Boyle et al., 2007). As the theoretical analysis is based on dimensionless distances, times, and velocities, the integral scale $\lambda_{\ln K}$ of the $\ln K$-fields is set to unity, and the velocity-fields in the numerical simulations are scaled such that the mean velocity is unity, too.

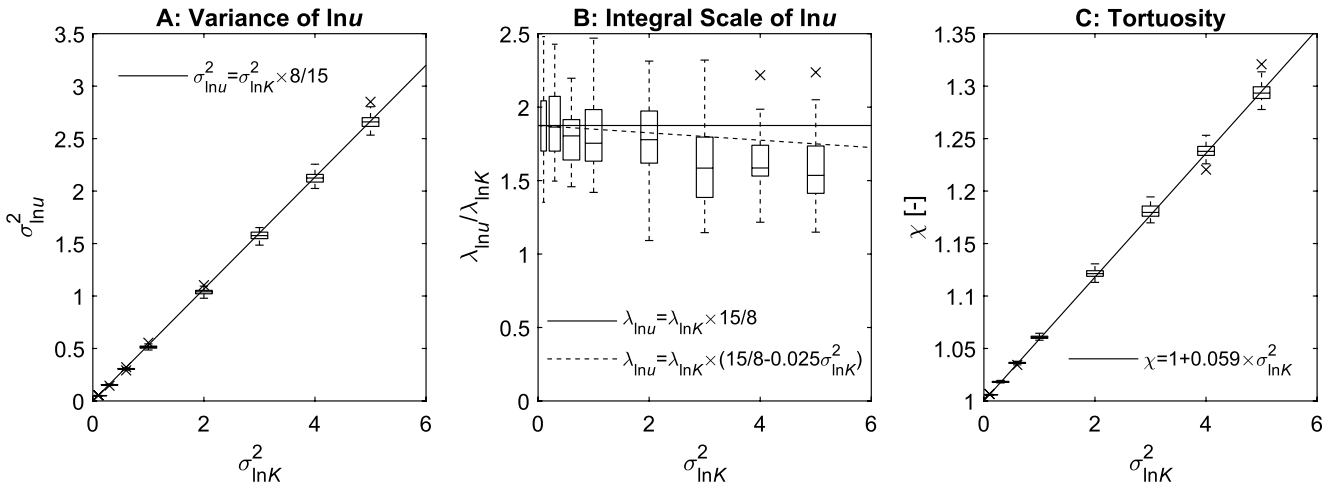

Figure 4. Variance and integral scale of the log-effective velocity, and tortuosity of the flow fields in 3-D periodic domains with isotropic exponential covariance function of log-hydraulic conductivity. Whisker boxes: results of 50 realizations obtained with Finite-Volume simulations; lines: linear trends as explained in the legends.

Particles are subsequently introduced at all cell-interfaces perpendicular to the x-direction in 50 starting planes with distance $0.8\lambda_{\ln K}$ to each other, resulting in 2×10^6 particles per realization. They are tracked by the semi-analytical approach of Pollock (1988), until they have passed 20 integral scales in the x-direction. For flux-weighted injection, the travel times of a particle observed at regular distances of $0.1\lambda_{\ln K}$ are weighted by the velocity of that particle at the injection point when computing metrics of travel-time distributions. The open-source code for flow and transport is written in Matlab (Cirpka, 2022), performing the flow simulations on the central processing unit, and particle tracking on the graphic processing unit (see also Hansen et al., 2018). In total we consider 50 realizations each for $\sigma^2_{\ln K}$-values of 0.1, 0.3, 0.6, 1, 2, 3, 4, and 5.

As outlined in Section 2.1, the effective velocity $u(\mathbf{x})$ at location $\mathbf{x}$ is not the longitudinal local velocity component v_x, because the latter may occasionally have negative values in simulations with high variances of $\ln K$. Instead it is defined as the absolute velocity scaled by the advective tortuosity, $\|\mathbf{v}\|_2/\chi$. The advective tortuosity compares the average length of streamlines to the linear distance between the starting and end point of trajectories (Ghanbarian et al., 2013; Koponen et al., 1996). In the average over all streamlines, it is exactly given by the ratio of the mean absolute velocity and the mean longitudinal velocity component (Comolli et al., 2019; Koponen et al., 1996):

$$\chi = \frac{\mu_{\|\mathbf{v}\|_2}}{\mu_{v_x}} = \mu_{\|\mathbf{v}\|_2} \tag{52}$$

We compute this property from the numerical Eulerian velocity field, in which the average is performed over all cell centers of the numerical grid. We then scale the local absolute velocity at the cell centers with the same tortuosity χ everywhere to obtain the effective velocity $u(\mathbf{x})$. The log-effective velocity fields $\ln u(\mathbf{x})$ are periodic and their covariance function can easily be evaluated by spectral analysis. Integral scales are reported in the direction of mean flow.

Figure 4 shows the empirical variance and integral scale of the log-effective velocity as a function of $\sigma^2_{\ln K}$. The boxplots describe the distributions over the 50 realizations by their median, interquartile range, range, and outliers. For 3-D isotropic media, linear stochastic theory predicts for small values of $\sigma^2_{\ln K}$ (e.g., Dagan, 1989; Gelhar, 1993):

$$\sigma^2_{\ln u} = \sigma^2_u \frac{8}{15} \sigma^2_{\ln K}. \tag{53}$$

which holds in this form because the velocity is normalized by $\mu_{v,u}$. The numerical results show an excellent agreement with this expression.

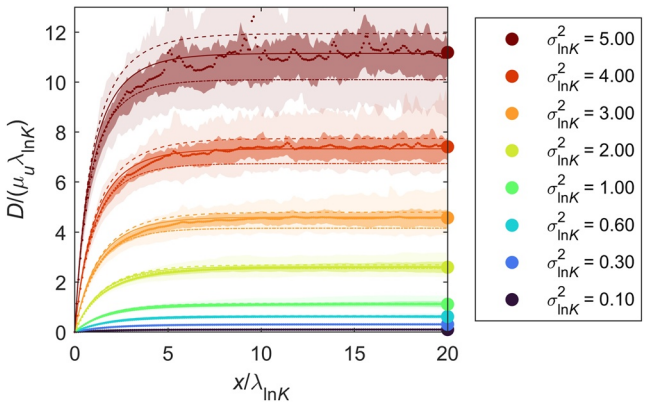

Figure 5. Dimensionless ensemble dispersion coefficient D according to Equation 36 as function of dimensionless distance. Comparison between 3-D ensemble-averaged particle-tracking simulations with injection into the flux (light shading: 90% confidence interval; dark shading: interquartile range; dots: mean over 50 realizations; markers: average value over the last 10 integral scales) and analytical results according to Equation 41 with $\sigma^2_{\ln u} = \frac{8}{15}\sigma^2_{\ln K}$ (lines). Dashed line: $\lambda_{\ln u} = \frac{15}{8}\lambda_{\ln K}$; dash-dotted line: $\lambda_{\ln u}$ according to the numerical findings shown in Figure 4B; solid line: $\lambda_{\ln u} = \left(\frac{15}{8} - 0.025\sigma^2_{\ln K}\right)\lambda_{\ln K}$.

The velocity integral scale λ_u for small values of $\sigma^2_{\ln K}$ can also be predicted from linear stochastic theory because the dimensionless asymptotic longitudinal effective dispersion coefficient D_∞ is (Gelhar & Axness, 1983):

$$D_\infty = \sigma_u^2 \lambda_u = \sigma^2_{\ln K}, \tag{54}$$

in which the dimensional dispersion coefficient is scaled with $\mu_{v,u}\lambda_{\ln K}$. The combination of Equations 53 and 54 leads to:

$$\lambda_u = \frac{15}{8}\lambda_{\ln K}. \tag{55}$$

At small variances $\sigma^2_{\ln K}$, the integral scale of u and $\ln u$ are approximately the same, $\lambda_{\ln u} \approx \lambda_u$. Figure 4b shows the empirical integral scales of $\ln u$ from the 3-D numerical simulations by the boxplots. They show large variations among the realizations, their averages are well described by the first-order result, but show a slight decrease with increasing $\sigma^2_{\ln K}$. Figure 4b also includes the empirical relationship:

$$\lambda_{\ln u} = \lambda_{\ln K}\left(\frac{15}{8} - 0.025\sigma^2_{\ln K}\right) \tag{56}$$

which is obtained by fitting the analytical expressions for $D(x)$ to the simulation data (see below).

Figure 4c shows the tortuosity χ as a function of $\sigma^2_{\ln K}$. Linear perturbation theory gives:

$$\chi = 1 + \frac{\sigma^2_{\ln K}}{15}, \tag{57}$$

which is slightly underestimated by the numerical data (slope of 0.059 rather than 0.067). The small difference may be explained by the numerical method of evaluating χ.

Figure 5 shows a comparison between distance-dependent dimensionless ensemble dispersion coefficients obtained by the numerical models for flux-weighted injection of the particles and predictions by the Spatial Markov Model according to Equation 41 assuming a volume-weighted variance of log-normalized velocity $\sigma^2_{\ln u} = \frac{8}{15}\sigma^2_{\ln K}$. The shaded areas represent the 90% and 50% confidence intervals over 50 realizations, and the dots the ensemble means. The large markers at $x = 20\lambda_{\ln K}$ denote the average values of the numerical results over the last 10 integral scales. The different line patterns indicate predictions by Equation 41 using different integral scales $\lambda_{\ln u}$ of log-velocity. Assuming a constant integral scale $\lambda_{\ln u} = \frac{15}{8}\lambda_{\ln K}$ (dashed lines), which is in agreement with linear theory at the limit of $\sigma^2_{\ln K} \to 0$, overestimates ensemble dispersion in cases of large log-conductivity variances. Taking the empirical findings of $\lambda_{\ln u}$ from the numerical results shown in Figure 4b (dash-dotted lines) underestimated ensemble dispersion. A good agreement is found with the empirical correction of $\lambda_{\ln u}$ by Equation 56, indicated in Figure 5 by solid lines.

4. Discussion and Conclusions

Spatial Markov Models provide an upscaled framework to describe solute transport in heterogeneous formations. Upon choosing the bivariate log-normal distribution as the joint distribution of slowness in two subsequent spatial transitions, the rules for propagating particles in the longitudinal direction are fully characterized by the mean Eulerian velocity of the flow field, by the variance, and by the integral scale of the log-Lagrangian velocity. Together with a choice of the injection mode, the parameterization can capture short- and large-distance mean travel times of particles and their variance.

The bivariate log-normal distribution considered here is a conceptual choice rather than the closed-form derivation from a particular model of hydraulic-conductivity fluctuations. Likewise, the first-order Markovian assumption of velocity transitions is the conceptual simplification of more complicated velocity covariance functions derived

in first order for second-order stationary log-conductivity fields (e.g., Russo, 1995, for 3-D fields). In as much, it cannot be expected that the model analyzed here can predict the exact shape by which the ensemble-dispersion coefficient evolves from the short- to the large-distance limit, but the agreement between the Spatial Markov Model and the numerical simulations is excellent.

In the limit of $\sigma^2_{\ln K} \to 0$, first-order perturbation approaches yield exact expressions of solute spreading in flow fields with uniform mean hydraulic gradient and second-order stationary log-conductivity field. Our expressions for the variance and integral scale of log-velocity are chosen such that the results of the Spatial Markov Model are in agreement with linear theory in the low-variance limit. In contrast to linear theory, however, they extend also to cases with high velocity variance. Even when using expressions for $\ln u$-statistics that directly relate to results of first-order theory, namely $\sigma^2_{\ln u} = \frac{8}{15}\sigma^2_{\ln K}$ and $\lambda_{\ln u} = \frac{15}{8}\lambda_{\ln K}$ for the case of isotropic heterogeneity, the estimate of the asymptotic ensemble dispersion coefficient is only about 10%–15% off at $\sigma^2_{\ln K} = 5$, whereas linear theory misses the correct value by a factor of about two. Our numerical results indicate that Equation 20 for the variance of log-velocity provides a robust estimate over the entire range of $\sigma^2_{\ln K}$-values considered, whereas the first-order expression for the integral scale requires a small correction at high values of $\sigma^2_{\ln K}$, given by the empirical Equation 56. With these results, we obtain a clear relationship between metrics of the log-conductivity statistics and the coefficients of the Spatial Markov Model, at least for the case of second-order stationary log-conductivity fields with isotropic covariance function.

In this study, we have exclusively considered ensemble dispersion for the case of advective transport. The Spatial Markov Model can also be applied to large-scale solute transport affected by local dispersion (Le Borgne et al., 2008). Toward this end both the marginal distribution of the travel-time increments and the statistical dependence of two subsequent increments must be modified from the strictly advective case. Going beyond predicting ensemble-averaged travel times of solute particles, by contrast, requires extra efforts. The approach, as discussed here, does not provide two-particle statistics needed to predict effective dispersion (e.g., Fiori & Dagan, 2000) or full statistical distributions of concentration (e.g., Fiorotto & Caroni, 2002; Fiorotto & Caroni, 2003). Approaches of extending Spatial Markov Models to account for mixing have been discussed by Sherman et al. (2021), but are beyond the scope of the present study.

Appendix A: Flux-Weighted Probability-Density Function of Log-Normal Distributed Velocity

We start with the definition of the flux-weighted distribution $p_f(u)$ of velocity and derive the following:

$$\begin{aligned} p_f(u) = \frac{u}{\mu_{v,u}} p_v(u) &= \frac{1}{\sqrt{2\pi\sigma^2_{\ln u}}} \exp\left(-\frac{(\ln u - \mu_{v,\ln u})^2}{2\sigma^2_{\ln u}}\right) \\ &= \frac{1}{\sqrt{2\pi\sigma^2_{\ln u}}} \exp\left(-\frac{(\ln u + \mu_{v,\ln u})^2 - 4\mu_{v,\ln u}\ln u}{2\sigma^2_{\ln u}}\right) \\ &= \frac{1}{\sqrt{2\pi\sigma^2_{\ln u}}} \exp\left(-\frac{(\ln u + \mu_{v,\ln u})^2}{2\sigma^2_{\ln u}}\right) \exp\left(\frac{4\mu_{v,\ln u}\ln u}{2\sigma^2_{\ln u}}\right). \end{aligned} \tag{A1}$$

We now use $\mu_{v,\ln u} = -\frac{1}{2}\sigma^2_{\ln u}$, resulting from $\mu_{v,u} = 1$, in the second exponential expression, yielding:

$$\begin{aligned} p_f(u) &= \frac{1}{\sqrt{2\pi\sigma^2_{\ln u}}} \exp\left(-\frac{(\ln u + \mu_{v,\ln u})^2}{2\sigma^2_{\ln u}}\right) \exp\left(-\frac{2\sigma^2_{\ln u}}{2\sigma^2_{\ln u}}\ln u\right) \\ &= \frac{1}{u\sqrt{2\pi\sigma^2_{\ln u}}} \exp\left(-\frac{(\ln u + \mu_{v,\ln u})^2}{2\sigma^2_{\ln u}}\right), \end{aligned} \tag{A2}$$

which confirms that the flux-weighted distribution $p_f(u)$ is log-normal with log-mean $\mu_{f,\ln u} = -\mu_{v,\ln u}$ and log-variance $\sigma^2_{\ln u}$, which is identical in the flux- and volume-weighted cases.

As the slowness is the inverse velocity, this identity implies that the flux-weighted slowness has the identical distribution as the volume-weighted velocity, and the volume-weighted slowness that of the flux-weighted velocity.

Data Availability Statement

The self-written Matlab codes are available at https://doi.org/10.5281/zenodo.6554308 under the international Creative Commons license CC-BY-NC 4.0. The HSL-MI20 algebraic multigrid (AMG) preconditioner used to solve the system of equations resulting from discretizing the flow equation is taken from the HSL library, a collection of Fortran codes for large-scale scientific computation (http://www.hsl.rl.ac.uk/catalogue/hsl_mi20.html).

Acknowledgments
This research has been supported by the German Research Foundation DFG under the grant Ci26/21-1. We thank three anonymous reviewers and the associate editor for their helpful comments. Open Access funding enabled and organized by Projekt DEAL.

References

Adams, E. E., & Gelhar, L. W. (1992). Field study of disperion in a heterogeneous aquifer 2. spatial moment analysis. *Water Resources Research*, *28*(12), 3293–3307. https://doi.org/10.1029/92wr01757

Ahmadi, A., Quintard, M., & Whitaker, S. (1998). Transport in chemically and mechanically heterogeneous porous media—V. Two-equation model for solute transport with adsorption. *Advances in Water Resources*, *22*(1), 59–86. https://doi.org/10.1016/S0309-1708(97)00032-8

Benson, D., Wheatcraft, S., & Meerschaert, M. (2000). Application of a fractional advection-dispersion equation. *Water Resources Research*, *36*(6), 1403–1412. https://doi.org/10.1029/2000WR900031

Berkowitz, B., Cortis, A., Dentz, M., & Scher, H. (2006). Modeling non-Fickian transport in geological formations as a continuous time random walk. *Reviews of Geophysics*, *44*(2), RG2003. https://doi.org/10.1029/2005RG000178

Berkowitz, B., & Scher, H. (1997). Anomalous transport in random fracture networks. *Physical Review Letters*, *79*(20), 4038–4041. https://doi.org/10.1103/physrevlett.79.4038

Boyle, J., Mihajlovic, M. D., & Scott, J. A. (2007). *HSL_MI20: An efficient AMG preconditioner*. (Tech. Rep. No. RAL-TR-2007-021). SFTC Rutherford Appleton Laboratory, Harwell Science and Innovation Campus. Retrieved from https://www.numerical.rl.ac.uk/reports/bmsRALTR2007021.pdf

Cherblanc, F., Ahmadi, A., & Quintard, M. (2003). Two-medium description of dispersion in heterogeneous porous media: Calculation of macroscopic properties. *Water Resources Research*, *39*(6), 1154. https://doi.org/10.1029/2002WR001559

Cirpka, O. A. (2022). Spatial Markov Model. *Zenodo*. https://doi.org/10.5281/zenodo.6554308

Comolli, A., Hakoun, V., & Dentz, M. (2019). Mechanisms, upscaling, and prediction of anomalous dispersion in heterogeneous porous media. *Water Resources Research*, *55*(10), 8197–8222. https://doi.org/10.1029/2019wr024919

Cvetkovic, V., Cheng, H., & Wen, X.-H. (1996). Analysis of nonlinear effects on tracer migration in heterogeneous aquifers using Lagrangian travel time statistics. *Water Resources Research*, *32*(6), 1671–1680. https://doi.org/10.1029/96WR00278

Cvetkovic, V., Fiori, A., & Dagan, G. (2014). Solute transport in aquifers of arbitrary variability: A time-domain random walk formulation. *Water Resources Research*, *50*(7), 5759–5773. https://doi.org/10.1002/2014WR015449

Cvetkovic, V., Shapiro, A. M., & Dagan, G. (1992). A solute flux approach in transport in heterogeneous formations : 2. Uncertainty analysis. *Water Resources Research*, *28*(5), 1377–1388. https://doi.org/10.1029/91WR03085

Dagan, G. (1984). Solute transport in heterogeneous porous formations. *Journal of Fluid Mechanics*, *145*(1), 151–177. https://doi.org/10.1017/S0022112084002858

Dagan, G. (1989). *Flow and transport in porous formations*. Springer Verlag.

Dagan, G., & Fiori, A. (1997). The influence of pore-scale dispersion on concentration statistical moments in transport through heterogeneous aquifers. *Water Resources Research*, *33*(7), 1595–1605. https://doi.org/10.1029/97wr00803

Dentz, M., Comolli, A., Hakoun, V., & Hidalgo, J. J. (2020). Transport upscaling in highly heterogeneous aquifers and the prediction of tracer dispersion at the MADE site. *Geophysical Research Letters*, *47*(22), e2020GL088292. https://doi.org/10.1029/2020GL088292

Dentz, M., Kang, P. K., Comolli, A., Le Borgne, T., & Lester, D. R. (2016). Continuous time random walks for the evolution of Lagrangian velocities. *Physical Review Fluids*, *1*(7), 074004. https://doi.org/10.1103/PhysRevFluids.1.074004

Dentz, M., Kinzelbach, H., Attinger, S., & Kinzelbach, W. (2000). Temporal behavior of a solute cloud in a heterogeneous porous medium 1. Point-like injection. *Water Resources Research*, *36*(12), 3591–3604. https://doi.org/10.1029/2000WR900162

Dietrich, C., & Newsam, G. (1993). A fast and exact method for multidimensional Gaussian stochastic simulations. *Water Resources Research*, *29*(8), 2861–2869. https://doi.org/10.1029/93wr01070

Doob, J. L. (1942). The Brownian movement and stochastic equations. *Annals of Mathematics*, *43*(2), 351–369. https://doi.org/10.2307/1968873

Englert, A., Vanderborght, J., & Vereecken, H. (2006). Prediction of velocity statistics in three dimensional multi-Gaussian hydraulic conductivity fields. *Water Resources Research*, *42*(W03418). https://doi.org/10.1029/2005WR004014

Fiori, A. (2001). The relative dispersion and mixing of passive solutes in transport in geologic media. *Transport in Porous Media*, *42*(1–2), 69–83. https://doi.org/10.1023/a:1006795910792

Fiori, A., & Dagan, G. (2000). Concentration fluctuations in aquifer transport: A rigorous first-order solution and applications. *Journal of Contaminant Hydrology*, *45*(1–2), 139–163. https://doi.org/10.1016/s0169-7722(00)00123-6

Fiorotto, V., & Caroni, E. (2002). Solute concentration statistics in heterogeneous aquifers for finite Peclet values. *Transport in Porous Media*, *48*(3), 331–351. https://doi.org/10.1023/a:1015744421033

Fiorotto, V., & Caroni, E. (2003). Solute concentration statistics in heterogeneous aquifers for finite Peclet values—Correction. *Transport in Porous Media*, *50*(3), 373.

Gelhar, L. W. (1993). *Stochastic subsurface hydrology*. Prentice-Hall.

Gelhar, L. W., & Axness, C. L. (1983). Three-dimensional stochastic analysis of macrodispersion in aquifers. *Water Resources Research*, *19*(1), 161–180. https://doi.org/10.1029/wr019i001p00161

Ghanbarian, B., Hunt, A., Ewing, R. P., & Sahimi, M. (2013). Tortuosity in porous media: A critical review. *Soil Science Society of America Journal*, *77*(5), 1461–1477. https://doi.org/10.2136/sssaj2012.0435

Gotovac, H., Cvetkovic, V., & Andricevic, R. (2009). Flow and travel time statistics in highly heterogeneousporous media. *Water Resources Research*, *45*(7), W07402. https://doi.org/10.1029/2008WR007168

Haggerty, R., Fleming, S. W., Meigs, L. C., & McKenna, S. A. (2001). Tracer tests in a fractured dolomite: 2. Analysis of mass transfer in single-well injection-withdrawal tests. *Water Resources Research*, *37*(5), 1129–1142. https://doi.org/10.1029/2000wr900334

Haggerty, R., & Gorelick, S. M. (1995). Multiple-rate mass transfer for modeling diffusion and surface reactions in media with pore-scale heterogeneity. *Water Resources Research*, *31*(10), 2382–2400. https://doi.org/10.1029/95wr10583

Hansen, S. K., Haslauer, C. P., Cirpka, O. A., & Vesselinov, V. V. (2018). Direct breakthrough curve prediction from statistics of heterogeneous conductivity fields. *Water Resources Research*, *54*(1), 271–285. https://doi.org/10.1002/2017WR020450

Hyman, J. D., & Dentz, M. (2021). Transport upscaling under flow heterogeneity and matrix-diffusion in three-dimensional discrete fracture networks. *Advances in Water Resources*, *155*, 103994. https://doi.org/10.1016/j.advwatres.2021.103994

Kang, P. K., Le Borgne, T., Dentz, M., Bour, O., & Juanes, R. (2015). Impact of velocity correlation and distribution on transport in fractured media: Field evidence and theoretical model. *Water Resources Research*, *51*(2), 940–959. https://doi.org/10.1002/2014wr015799

Koponen, A., Kataja, M., & Timonen, J. (1996). Tortuous flow in porous media. *Physical Review E*, *54*(1), 406–410. https://doi.org/10.1103/physreve.54.406

Le Borgne, T., Dentz, M., & Carrera, J. (2008). Spatial Markov processes for modeling Lagrangian particle dynamics in heterogeneous porous media. *Physical Review E*, *78*(2), 026308. https://doi.org/10.1103/PhysRevE.78.026308

Li, L., Zhou, H., & Gomez-Hernandez, J. J. (2011). Transport upscaling using multi-rate mass transfer in three-dimensional highly heterogeneous porous media. *Advances in Water Resources*, *34*(4), 478–489. https://doi.org/10.1016/j.advwatres.2011.01.001

Massoudieh, A., Dentz, M., & Alikhani, J. (2017). A spatial Markov model for the evolution of the joint distribution of groundwater age, arrival time, and velocity in heterogeneous media. *Water Resources Research*, *53*(7), 5495–5515. https://doi.org/10.1002/2017WR020578

Morales, V. L., Dentz, M., Willmann, M., & Holzner, M. (2017). Stochastic dynamics of intermittent pore-scale particle motion in three-dimensional porous media: Experiments and theory. *Geophysical Research Letters*, *44*(18), 9361–9371. https://doi.org/10.1002/2017gl074326

Neuman, S. P., Winter, C. L., & Newman, C. M. (1987). Stochastic theory of field-scale Fickian dispersion in anisotropic porous media. *Water Resources Research*, *23*(3), 453–466. https://doi.org/10.1029/wr023i003p00453

Noetinger, B., Roubinet, D., Russian, A., Le Borgne, T., Delay, F., Dentz, M., et al. (2016). Random walk methods for modeling hydrodynamic transport in porous and fractured media from pore to reservoir scale. *Transport in Porous Media*, *115*(2), 345–385. https://doi.org/10.1007/s11242-016-0693-z

Nowak, W., Schwede, R. L., Cirpka, O. A., & Neuweiler, I. (2008). Probability density functions of hydraulic head and velocity in three-dimensional heterogeneous porous media. *Water Resources Research*, *44*(8), W08452. https://doi.org/10.1029/2007wr006383

Pollock, D. W. (1988). Semianalytical computation of path lines for finite-difference models. *Ground Water*, *26*(6), 743–750. https://doi.org/10.1111/j.1745-6584.1988.tb00425.x

Puyguiraud, A., Gouze, P., & Dentz, M. (2019). Upscaling of anomalous pore-scale dispersion. *Transport in Porous Media*, *128*(2), 837–855. https://doi.org/10.1007/s11242-019-01273-3

Russo, D. (1995). On the velocity covariance and transport modeling in heterogeneous anisotropic porous formations. 2. unsaturated flow. *Water Resources Research*, *31*(1), 139–145. https://doi.org/10.1029/94wr01784

Shapiro, A. M., & Cvetkovic, V. D. (1988). Stochastical analysis of solute arrival time in heterogeneous porous media. *Water Resources Research*, *24*(10), 1711–1718. https://doi.org/10.1029/wr024i010p01711

Sherman, T., Engdahl, N. B., Porta, G., & Bolster, D. (2021). A review of spatial Markov models for predicting pre-asymptotic and anomalous transport in porous and fractured media. *Journal of Contaminant Hydrology*, *236*, 03734. https://doi.org/10.1016/j.jconhyd.2020.103734

Stüben, K. (2001). A review of algebraic multigrid. *Journal of Computational and Applied Mathematics*, *128*(1–2), 281–309. https://doi.org/10.1016/s0377-0427(00)00516-1

Zerovnik, G., Trkov, A., Smith, D. L., & Capote, R. (2013). Transformation of correlation coefficients between normal and lognormal distribution and implications for nuclear applications. *Nuclear Instruments and Methods in Physics Research Section A: Accelerators, Spectrometers, Detectors and Associated Equipment*, *727*, 33–39. https://doi.org/10.1016/j.nima.2013.06.025